Atomic-Scale Spin-Polarized Scanning Tunneling Microscopy Applied to $Mn_3N_2(010)$

Haiqiang Yang and Arthur R. Smith*
Condensed Matter and Surface Science Program, Department of Physics and Astronomy, Ohio University, Athens, Ohio 45701

Margarita Prikhodko and Walter R. L. Lambrecht
Department of Physics, Case Western Reserve University, Cleveland, Ohio 44106-7079
(Received 31 March 2002; published 6 November 2002)

Atomic-scale spin-polarized scanning tunneling microscopy is demonstrated in the case of the unique surface spin structure of $Mn_3N_2(010)$ at 300 K. We find that the surface spin structure is manifested as a modulation of the normal atomic row height profile. The atomic-scale spin-polarized image is thus shown to contain two components, one the normal, nonpolarized part, and the other the magnetic, spin-polarized part. A method is presented for separating these two spatially correlated components, and the results are compared with simulations based on integrated local spin density of states calculated from first principles.

DOI: 10.1103/PhysRevLett.89.226101 PACS numbers: 68.37.Ef, 68.35.Bs, 75.50.Ee, 75.70.Rf

While the electron's charge has been the basis for modern science and technology, the challenge of the future is to utilize the electron's spin [1]. For magnetic materials, it is of great interest to correlate spin and chemical structure with the highest possible spatial resolution. Wiesendanger *et al.* have reported the use of spin-polarized scanning tunneling microscopy (SP-STM) for measuring magnetic surface structure, using either ferromagnetic (FM) or antiferromagnetic (AFM)-coated STM tips, even demonstrating atomic-scale spin contrast for a 1×1 AFM monolayer of Mn atoms [2–4]. Thus, SP-STM has been shown to be a powerful spin imaging technique.

Interestingly, however, Heinze *et al.* reported that the constant current (CC) mode atomic-scale spin-polarized image was dominated by the magnetic component, with no chemical contrast [4]. In this Letter, we show that both the magnetic *and* the nonmagnetic atomic-scale information *can* be obtained *simultaneously* in the CC mode using SP-STM. We also demonstrate a separation procedure resulting in profiles which can be compared with model calculations of the magnetic and nonmagnetic integrated local density of states (ILDOS).

The SP-STM experiments are performed in an ultrahigh vacuum (UHV) analysis chamber connected to a molecular beam epitaxy (MBE) growth chamber. We study $Mn_3N_2(010)$, a magnetic transition metal nitride surface, which we prepare using a solid source effusion cell for Mn and a rf plasma source for N [5,6]. All STM imaging is performed at 300 K in CC mode. For normal STM measurements, we use W tips which are cleaned in UHV by electron bombardment. For SP-STM measurements, we coat the cleaned W tips *in situ* at 300 K with either (i) 5–10 ML of Mn, or (ii) 5–10 ML of Fe. While the Néel temperature of Mn is only $\sim$100 K [7], spin-polarized photoelectron diffraction of thin films of Mn have shown spin asymmetry up to $\sim$500 K, which was attributed to the surface atoms [8]. The Fe-coated tips (T_c of Fe is 1043 K) are magnetized in the direction normal to the tip axis in a 40 mT field.

The bulk structure of Mn_3N_2 is well known [9–11]. It has a face-centered tetragonal (fct) rocksalt-type structure. The bulk magnetic moments of the Mn atoms are FM within (001) planes, lie along the [100] direction, and are layerwise AFM along [001]. The bulk Néel point of Mn_3N_2 is 925 K [9]. Besides the magnetic superstructure, every third (001) layer along the c direction has all N sites vacant. This results in a bulk unit cell having $c = 12.13$ Å (six atomic layers).

Using MBE, we grow atomically smooth layers of Mn_3N_2 with the c axis parallel to the growth surface, which is (010) [5,6]. The magnetic structure of our sample has been characterized by neutron scattering and shows a clear magnetic peak originating from the layerwise AFM structure [5]. Shown in Fig. 1(a) is a STM image of this surface acquired using a W tip (sample bias $V_s = -0.4$ V, tunnel current $I_t = 0.4$ nA), revealing an atomic-scale row structure with row spacing $= c/2 = 6.06$ Å, the spacing between N-vacancy planes. Because the film is grown on a fourfold symmetric substrate —MgO(001), two types of domains occur.

With a very sharp tip, individual Mn atoms can be resolved, as shown in Fig. 1(b) ($V_s = -0.3$ V, $I_t = 0.3$ nA). The image is a perfect match with the Mn atom sublattice shown in Fig. 1(c), where the higher and lower maxima correspond to the Mn(1) and Mn(2) atoms, respectively. The measured height difference between Mn(1) and Mn(2) atoms is 0.07 Å, which is attributed to surface relaxation. Little bias dependence of the atomic resolution image shows that this surface has metallic character, consistent with our calculations [12]. The surface geometrical unit cell, containing six Mn atoms and four N atoms (3 : 2 ratio), can be denoted as $c(1 \times 1)$, whereas the surface magnetic unit cell is just 1×1 (since $\mu_{\mathrm{Mn}(1)} \neq \mu_{\mathrm{Mn}(2)}$).

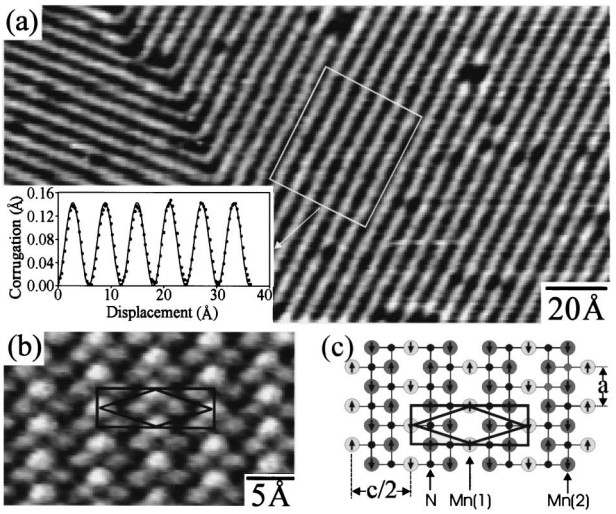

FIG. 1. (a) STM image of $Mn_3N_2(010)$ surface acquired at $V_s = -0.4$ V and $I_t = 0.4$ nA. The inset shows the average line profile (data points) over the indicated region. The solid line is a sinusoid fitted to the data. (b) Atomic resolution STM image acquired at $V_s = -0.3$ V and $I_t = 0.3$ nA. (c) Bulk terminated surface model. The $c(1 \times 1)$ geometrical unit cell and 1×1 magnetic unit cell are indicated by the black rhombus and black rectangle, respectively.

Shown in Fig. 2(a) is a SP-STM image of the surface acquired using a Mn-coated W tip ($V_s = -0.6$ V, $I_t = 0.8$ nA) in which the row structure (with period $= c/2$) is observed, but, in addition, a modulation (with period $= c$) of the height of the rows is also clearly observed. As shown in Fig. 2(b), the modulation is clearly evident for both domains D1 and D2 by the area-averaged line profiles taken from inside the boxed regions on either side of the domain boundary. The darkening observed near the domain wall is a different effect also seen in some normal STM images [5], to be discussed elsewhere.

According to Wortmann *et al.* [13], the tunneling current can be written as the sum of a non-spin-polarized component I_o proportional to the local density of states (LDOS) of the tip n_T and the sample integrated LDOS (ILDOS), $\tilde{n}_S = \int [f(\epsilon\text{-}\epsilon_F) - f(\epsilon\text{-}\epsilon_F\text{-eV})] n_S(\epsilon) d\epsilon$, where f is the Fermi function, and a spin-polarized component I_P proportional to the projection of the magnetic LDOS of the tip $\mathbf{m}_T$ onto the magnetic ILDOS of the sample $\tilde{\mathbf{m}}_S$:

$$I_T = I_o + I_P \sim n_T \tilde{n}_S + \mathbf{m}_T \cdot \tilde{\mathbf{m}}_S. \quad (1)$$

The change of the tunneling current,

$$\Delta I_T \sim z(\mathbf{R}_T) \sim n_T \tilde{n}_S(\mathbf{R}_T) + m_T \tilde{m}_S(\mathbf{R}_T) \cos\theta(\mathbf{R}_T) - C, \quad (2)$$

where C is a constant and $\mathbf{R}_T$ is the (x, y) position of the tip. When m_T and $\tilde{m}_S$ are both nonzero, the second term in Eq. (2) will vary with the angle θ on a local atomic scale, resulting in the height modulation as observed in Fig. 2.

As further confirmation of the spin-polarized modulation mechanism, we notice in Fig. 2(b) the clear difference in modulation amplitude on the two sides of the domain boundary, as expected from the cosine dependence of the magnetic component. For the domain D1 (red line), the modulation amplitude is about a factor of 2 larger than for the domain D2 (blue line). Since the height modulation is proportional to $m_T \tilde{m}_S \cos\theta$ [see Eq. (4) below], then it is simple to show that

$$\theta = \arctan(\Delta z_2 / \Delta z_1), \quad (3)$$

where Δz_1 and Δz_2 are the height modulation in domains D1 and D2, respectively. In the case shown here with $\Delta z_1 \approx 0.04$ Å and $\Delta z_2 \approx 0.02$ Å, we find $\theta \approx 27°$.

We also notice from Fig. 2(b) that a high peak (H) on one side of the domain boundary converts to a low peak (L) on the other side. This inversion is simulated in Fig. 2(c) by a simple AFM model configuration of spin moments and a tip spin at the angle $\theta = 27°$. The gray scale for each magnetic atom is proportional to $m_T \tilde{m}_S \cos\theta$ (white: $\theta = 0$; black: $\theta = \pi$). Clearly, the

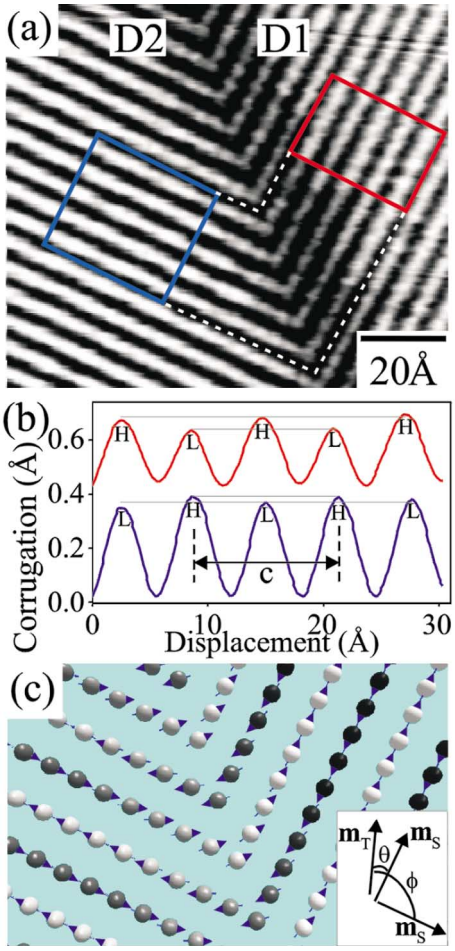

FIG. 2 (color). (a) SP-STM image acquired using a Mn-coated W tip at $V_s = -0.6$ V and $I_t = 0.8$ nA. (b) Two area-averaged line profiles (red and blue) corresponding to the regions inside the red and blue rectangles in (a). (c) Simulated SP-STM map: contrast: white ↔ black ⇒ θ: $0 \leftrightarrow \pi$. The inset shows the moments of tip ($\mathbf{m}_T$) and the sample ($\mathbf{m}_S$) for the two different domains and the angles between them. Each ball represents a magnetic atom.

inversion occurs when the difference $\phi - \theta = \pi/2$, where θ and ϕ are the two different angles between tip and sample moments in domains D1 and D2, respectively.

Next, we present a straightforward method of separating the magnetic and nonmagnetic components from the SP-STM data. Beginning with the SP-STM image shown in Fig. 3(a) ($V_s = -0.6$ V, $I_t = 0.8$ nA), we plot the average height profile $z(x)$, where x is along [001] [Fig. 3(b), dark blue line] and also $z(x + c/2)$ [Fig. 3(b), light blue line]. Clearly, by taking the difference and sum of these two functions, we extract the magnetic component with periodicity c and the nonmagnetic component with period $c/2$:

$$m_T \tilde{m}_S(x) \cos[\theta(x)] \sim [z(x) - z(x + c/2)]/2, \quad (4)$$

$$n_T \tilde{n}_S(x) \sim [z(x) + z(x + c/2)]/2 + C. \quad (5)$$

This is further justified if we assume that the bulk magnetic symmetry is maintained at the surface. Using this procedure, the resulting magnetic profile for the data of Fig. 3 has period $= c$ and a trapezoid-wave shape, as shown in Fig. 3(c) (violet line). The nonmagnetic profile is also shown in Fig. 3(c) (red line) having period $= c/2$ and a sinusoidal shape, the same as for the average line profile acquired with a nonmagnetic tip [Fig. 1(a)]. We note that the magnetic component amplitude is about 20% of the nonmagnetic component amplitude.

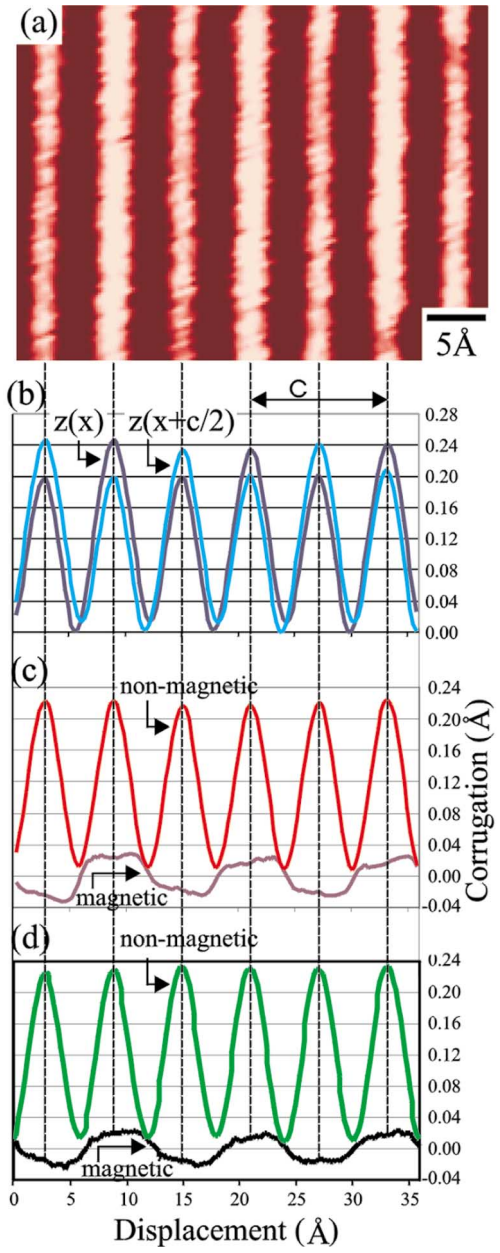

FIG. 3 (color). (a) SP-STM image acquired using a Mn-coated W tip at a $V_s = -0.6$ V and $I_t = 0.8$ nA. (b) Area-averaged line profile $z(x)$ of the whole image of (a) (dark blue), and $z(x + c/2)$ (light blue). (c) The resulting nonmagnetic component (red) and magnetic component (violet) for the Mn-coated tip. (d) Nonmagnetic (green) and magnetic (black) components for the Fe-coated tip on a similar sample region.

We can rule out alternative explanations for the observed height modulation such as charge redistribution and asymmetric *d-d* orbital tunneling. In the absence of surface reconstruction, the surface primitive lattice translation vector is $\mathbf{c}/2 + \mathbf{a}/2$. This implies that the Mn(1) atoms in subsequent rows are completely equivalent in charge and orbitals. One does not expect a surface reconstruction because of the simple octahedral bonding, and none is observed.

To further support the magnetic origin of the effects reported here, the experiments were repeated with many (> 6) samples with many (> 9) tips (both Fe and Mn coated). The success rate for magnetic-coated tips is $\sim$50%. Shown in Fig. 3(d) are results (obtained) using an Fe-coated tip at similar tunneling parameters ($V_s = -0.4$ V, $I_t = 0.4$ nA) as for the Mn-coated tip. The nonmagnetic (green) and magnetic (black) line profiles are very similar to those obtained using the Mn-coated tip.

One might question why the magnetic components extracted in Figs. 3(c) and 3(d) do not show a layer by layer alternation or a simple sinusoidal form. First, we observe that shorter period fluctuations in the magnetic component at period $c/3$ (every two atomic layers) correspond to a larger reciprocal wave vector $\mathbf{G}$ in a 2D-Fourier analysis and that, according to Wortmann *et al.* [13], the current fluctuation decays exponentially with the magnitude of the reciprocal lattice vector. Thus, the image is dominated by the smallest nonzero $\mathbf{G}$ components unless the tip is extremely close to the surface. Of course, the $c/2$ periodic nonmagnetic component may still be stronger than the magnetic component.

Second, we can explain the trapezoid shape of the magnetic component by simulating the magnetic part of the height profile $[z_P(x)]$ as an exponentially weighted sum over surface atoms, as

$$z_P(x) \sim \sum m_T \tilde{m}_S(\mathbf{R}_i) \cos\theta_i e^{-2\kappa|\mathbf{R}_T - \mathbf{R}_i|}. \quad (6)$$

A similar equation is used to simulate the nonmagnetic part, replacing the prefactors of the exponential by $n_T \tilde{n}_S(\mathbf{R}_i)$. The outward relaxation of the Mn(1) as

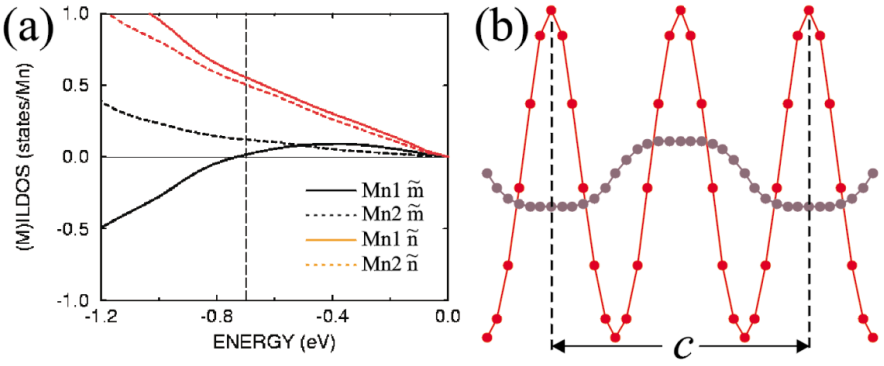

FIG. 4 (color). (a) $\tilde{m}_S$ and $\tilde{n}_S$ for Mn(1) and Mn(2) vs energy; (b) simulated magnetic (violet) and nonmagnetic (red) height profiles.

determined from the nonmagnetic STM is taken into account and the sum is converged by including 13 atomic rows. Prefactors were obtained from bulk spin-polarized integrated LDOS calculations, which were performed using a full-potential linear muffin-tin orbital method [14] in the local spin density functional approximation [15]. The results for the relevant energy window (-1.2 to 0 eV) are plotted in Fig. 4(a) which shows the net occupied magnetic ILDOS ($\tilde{m}_S$) and the occupied ILDOS ($\tilde{n}_S$) for Mn(1) and Mn(2). For the simulation, values for $\tilde{m}_{\mathrm{Mn1}}$, $\tilde{m}_{\mathrm{Mn2}}$, $\tilde{n}_{\mathrm{Mn1}}$, and $\tilde{n}_{\mathrm{Mn2}}$ of 0.02, 0.12, 0.56, and 0.51 states/atom were obtained at an energy of -0.7 eV.

Shown in Fig. 4(b) are the simulation results for a tip-atom–sample-atom center-to-center distance of 5 Å and $\kappa = 1.1$ Å^{-1}. Clearly, both the magnetic and the nonmagnetic simulated height profiles are in excellent agreement with the experimental ones. Moreover, the magnetic:nonmagnetic amplitude ratio was made to agree with the experiment by adjusting the spin polarization of the tip, $P_T \equiv m_T/n_T$, thus determining P_T to be 10.4%.

Thus, we find that the trapezoid profile is consistent with the layerwise AFM ordering, resulting from the small magnitude of $\tilde{m}_S$ (Mn1) compared to $\tilde{m}_S$ (Mn2) within a window of negative sample bias. The experiment does not imply, for instance, a surface reconstructed spin ordering ↑↑↑↓↓↓ in which the surface Mn(1) or Mn(2) moments are flipped. In fact, calculations show that the bulk ↑↑↑↓↓↓ model is 0.125 eV per Mn atom higher in energy than the bulk ↑↓↑↓↑↓ model [12]. At positive sample bias, $\tilde{m}_{\mathrm{Mn1}}$ is positive while $\tilde{m}_{\mathrm{Mn2}}$ is negative, and the experiment finds a reversal of the magnetic contrast.

In conclusion, we have applied atomic-scale SP-STM in the CC mode to study a transition metal nitride surface —$Mn_3N_2(010)$— and have clearly observed modulation of the normal row height profile. The reproducible observations with different magnetic tips unambiguously demonstrate that only a spin-polarization effect can explain these results. Furthermore, this spin-polarization effect is a natural explanation in terms of the known bulk ordering of the magnetic moments of Mn_3N_2. We have also demonstrated a method for separating the magnetic and nonmagnetic components of the height profile. These profiles are shown to agree well with simulations based on first-principles calculations.

This work is supported by the National Science Foundation under Grant No. 9983816. H. Yang acknowledges support by the Ohio University Postdoctoral Fellowship program. Special thanks also go to M.-Y. Chen for writing the SP-STM magnetic contrast simulation program and E. Hunt and S. Ulloa for careful manuscript reading and suggestions. The work at CWRU is supported by the Office of Naval Research.

*Corresponding author.
Electronic address: smitha2@ohio.edu

[1] S. A. Wolf *et al.*, Science **294**, 1488 (2001).
[2] R. Wiesendanger *et al.*, Phys. Rev. Lett. **65**, 247 (1990); R. Wiesendanger *et al.*, Science **255**, 583 (1992).
[3] A. Kubetzka, M. Bode, O. Pietzsch, and R. Wiesendanger, Phys. Rev. Lett. **88**, 057201 (2002).
[4] S. Heinze, M. Bode, A. Kubetzka, O. Pietzsch, X. Nie, S. Blügel, and R. Wiesendanger, Science **288**, 1805 (2000).
[5] H. Yang *et al.*, Appl. Phys. Lett. **78**, 3860 (2001).
[6] H. Yang, H. Al-Brithen, E. Trifan, D. C. Ingram, and A. R. Smith, J. Appl. Phys. **91**, 1053 (2002).
[7] D. H. Martin, *Magnetism in Solids* (Iliffe Books Ltd., London, 1967), p. 67.
[8] A. M. Keen, S. H. Baker, C. Binns, S. N. Mozley, C. Norris, and H. S. Derbyshire, Solid State Commun. **107**, 523 (1998).
[9] M. Tabuchi, M. Takahashi, and F. Kanamaru, J. Alloys Compd. **210**, 143 (1994).
[10] H. Jacobs and C. Stüve, J. Less-Common Met. **96**, 323 (1984); G. Kreiner and H. Jacobs, J. Alloys Compd. **183**, 345 (1992).
[11] A. Leineweber, R. Niewa, H. Jacobs, and W. Kockelmann, J. Mater. Chem. **10**, 2827 (2000).
[12] M. Prikhodko and W. R. L. Lambrecht, Bull. Am. Phys. Soc. **47**, 797 (2002); (unpublished).
[13] D. Wortmann, S. Heinze, Ph. Kurz, G. Bihlmayer, and S. Blügel, Phys. Rev. Lett. **86**, 4132 (2001).
[14] M. Methfessel, M. van Schilfgaarde, and R. A. Casali, in *Electronic Structure and Physical Properties of Solids: The Uses of the LMTO Method*, edited by Hugues Dreyssé, Lecture Notes in Physics (Springer-Verlag, Berlin, 2000), p. 114–147.
[15] U. von Barth and L. Hedin, J. Phys. C **5**, 2064 (1972).